

# Elevation Angle-Dependent 3D Trajectory Design for Aerial RIS-aided Communication

Yifan Liu, *Student Member, IEEE*, Bin Duo, *Member, IEEE*, Qingqing Wu, *Senior Member, IEEE*, Xiaojun Yuan, *Senior Member, IEEE*, Jun Li, *Senior Member, IEEE*, and Yonghui Li, *Fellow, IEEE*

**Abstract**—This paper investigates an aerial reconfigurable intelligent surface (RIS)-aided communication system under the probabilistic line-of-sight (LoS) channel, where an unmanned aerial vehicle (UAV) equipped with an RIS is deployed to assist two ground nodes in their information exchange. An optimization problem with the objective of maximizing the minimum average achievable rate is formulated to jointly design the communication scheduling, the RIS's phase shift, and the three-dimensional (3D) UAV trajectory. To solve such a non-convex problem, we propose an efficient iterative algorithm to obtain its suboptimal solution. Simulation results show that our proposed design significantly outperforms the existing schemes and provides new insights into the elevation angle and distance trade-off for the UAV-borne RIS communication system.

**Index Terms**—UAV communication, reconfigurable intelligent surface, probabilistic LoS channel, trajectory design.

## I. INTRODUCTION

Besides terrestrial deployment, wireless networks are gradually evolving into air-ground integrated networks to achieve ubiquitous wireless connection and network capacity upgrades [1], [2]. Recently, unmanned aerial vehicles (UAVs) have obtained substantial attention in wireless communication. Thanks to their high mobility, low cost, and line-of-sight (LoS) transmission, UAVs can further improve communication coverage, throughput, and average secrecy rates [3]–[5].

Recently, the reconfigurable intelligent surface (RIS) has attracted considerable attention due to its low profile, low energy consumption, and ability to overcome the non-LoS (NLoS) transmission [6]. Typically, the RIS contains many reflective elements, each of which is manipulated to induce changes in the amplitude and phase shift of incident signals to create favorable propagation environment. The RIS becomes a promising technology for the future mobile communications. It can solve the pain points of fifth-generation (5G), such as high energy consumption and coverage voids. By optimizing the phase shift of all elements of the RIS, the signals from different transmission paths can be precisely aligned at the desired receiver to increase the signal power [7].

For typical application scenarios of UAV communications in urban areas, such as cargo delivery, traffic monitoring, and so on, their communication links are often blocked by tall building, which leads to severe degradation of channel quality. Fortunately, with its low power consumption and lightweight, the RIS can be installed at an appropriate location to reconfigure the propagation environment of air-ground links, thereby improving communication performance. Several works have studied various RIS-assisted UAV communication systems. In general, these studies mainly fall into two categories, one for terrestrial RIS [8]–[11] and the other for aerial RIS [12]–[16]. In particular, for the first category, the UAV trajectory and the phase shift of the RIS mounted on building facades are jointly designed to optimize different objectives such as communication coverage [8], energy efficiency [9], confidentiality [10], and communication rates [11].

Taking advantage of the UAV's ability to fly freely in the three-dimensional (3D) space, the RIS can be mounted on the UAV. This allows the RIS to fly along with the UAV, which is more flexible in adjusting its 3D location than the conventional terrestrial RIS, thus enhancing communication services [12], [13]. An aerial RIS was deployed in [14] to expand the coverage of communication services, where the worst-case signal-to-noise ratio (SNR) was improved by jointly optimizing the transmit beamforming, the RIS's placement, and the 3D passive beamforming. In [15], multiple users were served by a base station (BS), and their received powers were significantly enhanced with the aid of an aerial RIS. To provide communication services for blocked users that locate far apart while preventing information leakage, the UAV equipped with one RIS was deployed in [16] to improve the security and energy efficiency. Above works only took the ideal deterministic LoS channel (DLC) into account, which has two limitations in practice. *i)* The DLC model cannot fully capture the critical effects of the UAV location-dependent LoS and NLoS states in urban areas with typically high and dense buildings/trees [17]; *ii)* the DLC model cannot accurately describe the elevation angle and distance trade-off, since the elevation angles between the UAV and ground nodes (GNs) are closely related to the 3D UAV trajectory [18]. Therefore, it is intuitive that the UAV trajectory designed under the simplified DLC model will undoubtedly cause significant performance loss in practical urban environments.

Motivated by the above, this paper considers an aerial RIS-aided communication system, where the UAV-borne RIS assists in information exchange with two GNs. In particular, we adopt a more accurate probabilistic LoS channel (PLC) model to characterize the complex channel states of LoS and NLoS in an urban environment. To maximize the minimum

Yifan Liu is with the College of Mechanical and Electrical Engineering, Chengdu University of Technology, Chengdu 610059, China. Bin Duo is with the College of Computer Science and Cyber Security, Chengdu University of Technology, Chengdu 610059, China. Qingqing Wu is with the State Key Laboratory of Internet of Things for Smart City, University of Macau, Macao 999078, China. Xiaojun Yuan is with the National Key Laboratory of Science and Technology on Communications, University of Electronic Science and Technology of China, Chengdu 611731, China. Jun Li is with the School of Electronic and Optical Engineering, Nanjing University of Science and Technology, Nanjing 210094, China. Yonghui Li is with the School of Electrical and Information Engineering, The University of Sydney, Sydney, NSW 2006, Australia.

average achievable rate, we jointly optimize the communication scheduling, the RIS's phase shift, and the 3D UAV trajectory. The formulated problem is non-convex and difficult to solve, since it contains intractable non-convex constraints, binary scheduling variables, and the complicated achievable rate expression concerning UAV trajectory variables. To tackle such challenges, we propose an efficient iterative algorithm to obtain a high-quality solution. Simulation results show that our proposed joint design for the aerial RIS-aided communication system under the PLC model can significantly improve the max-min rate compared to that under the conventional DLC model. This is because the optimized UAV trajectory better balances the elevation angle and distance trade-off, resulting in the enhanced gain of the cascaded channel between the UAV and the GNs.

Note that although the authors in [19] and [20] also considered a UAV-borne RIS communication system under the PLC model, in this paper, both the system model and the proposed algorithm are different, which results in the fundamental trade-off between the elevation angle and distance for rate enhancement. Furthermore, in [17], the 3D UAV trajectory was designed for data collection under the PLC model; however, this paper considers a new UAV-borne RIS communication system and derives a new expression for the expected achievable rate function.

## II. SYSTEM MODEL AND PROBLEM FORMULATION

In this paper, we consider an aerial RIS-aided communication system, where two GNs exchange information via a UAV-borne RIS<sup>1</sup> due to the blockage of dense buildings. We characterize the position of the UAV and the two GNs via the 3D Cartesian coordinate system. It is assumed that the UAV flies over a given duration  $T$  to assist in reflecting signals via the RIS between the GNs, whose locations are denoted by  $\mathbf{w}_k = [x_k, y_k]$ ,  $k \in \mathcal{K} = \{1, 2\}$ . To ease the 3D UAV trajectory design,  $T$  is divided into  $N$  time slots that are equal in length, i.e.,  $T = N\delta_t$ , where  $\delta_t$  is the length of each time slot. Thus, the trajectory of the UAV can be approximated by a 3D sequence  $\{(\mathbf{q}[n], h[n])\}$ ,  $n \in \mathcal{N} = \{1, 2, \dots, N\}$ , where the discrete way-points  $\mathbf{q}[n] = [x[n], y[n]]$  and  $h[n]$  represent the horizontal and vertical locations, which satisfy the following constraints:

$$\|\mathbf{q}[n+1] - \mathbf{q}[n]\|^2 \leq \hat{\Omega}^2, \forall n, \quad (1)$$

$$\mathbf{q}[N+1] = \mathbf{q}_F, \mathbf{q}[1] = \mathbf{q}_0, \quad (2)$$

$$|h[n+1] - h[n]|^2 \leq \tilde{\Omega}^2, H_{\min} \leq h[n] \leq H_{\max}, \forall n, \quad (3)$$

where  $\mathbf{q}_0$  and  $\mathbf{q}_F$  denote the initial and final horizontal positions of the UAV, respectively,  $\hat{\Omega} = \hat{v}_{\max}\delta_t$  and  $\tilde{\Omega} = \tilde{v}_{\max}\delta_t$  are the maximum horizontal and vertical distance that the UAV can reach in each time slot, respectively, and  $\hat{v}_{\max}$  and  $\tilde{v}_{\max}$  are the corresponding maximum horizontal and vertical flying

speed of the UAV, respectively. Furthermore,  $H_{\min}$  and  $H_{\max}$  indicate the minimum and maximum altitude that the UAV can reach at any given time.

We assume that both GN 1 and GN 2 are equipped with an omni-directional single antenna. The RIS is equipped with a uniform planar array (UPA) of  $M = M_x \times M_y$  ( $M_x$  rows and  $M_y$  columns) reflective elements, each of which can be manipulated by an embedded development board, such as Raspberry Pi 4, mounted on the UAV. Since the UAV and the RIS are assembled compactly, we assume that their 3D coordinates are identical, causing negligible performance loss due to high flying altitude of the UAV [16]. We denote  $\Theta[n] = \text{diag}\{e^{j\theta_{1,1}[n]}, e^{j\theta_{1,2}[n]}, \dots, e^{j\theta_{M_x, M_y}[n]}\}$  as the diagonal phase-shift matrix of the RIS in the  $n$ th time slot, where  $\theta_{m_x, m_y}[n] \in [0, 2\pi)$  is the phase shift of  $m_x$ -th row and  $m_y$ -th column in the  $n$ th time slot, where  $m_x \in \mathcal{M}_x = \{1, \dots, M_x\}$  and  $m_y \in \mathcal{M}_y = \{1, \dots, M_y\}$ . Assume that the phase shift of each element is continuously controllable, which should satisfy  $|e^{j\theta_{m_x, m_y}[n]}| = 1$ .

To accurately represent the channel states in urban environments, we adopt the PLC model [22], for which the ground-UAV channel can be represented by LoS or NLoS state. Thus, for GN  $k$ , the LoS probability in the  $n$ th time slot is given by

$$P_k^L[n] = \frac{1}{1 + ae^{(-b[\psi_k[n]-a])}}, \quad (4)$$

where  $a > 0$  and  $b > 0$  are constants specified by the actual environment, and

$$\psi_k[n] = \frac{180}{\pi} \arctan\left(\frac{h[n]}{\|\mathbf{q}[n] - \mathbf{w}_k\|}\right) \quad (5)$$

is the elevation angle from GN  $k$  to the UAV in the  $n$ th time slot. The relevant NLoS probability can then be acquired as  $P_k^N[n] = 1 - P_k^L[n]$ . The channel gain between GN  $k$  and the UAV conditioned on the LoS state in the  $n$ th time slot can be expressed as

$$\mathbf{h}_k^L[n] = \tau[n] \left[ 1, \dots, e^{-j\frac{2\pi d}{\lambda}(M_x-1)\sin\varphi_k[n]\cos\omega_k[n]} \right]^T \otimes \left[ 1, \dots, e^{-j\frac{2\pi d}{\lambda}(M_y-1)\sin\varphi_k[n]\sin\omega_k[n]} \right]^T, \quad (6)$$

where  $\tau[n] = \sqrt{\beta_0 d_k^{-\alpha_L}[n]}$ ,  $\beta_0$  is the path loss at the reference distance of  $D_0 = 1$  meter (m),  $d_k[n] = \sqrt{(\mathbf{q}[n] - \mathbf{w}_k)^2 + h[n]^2}$  is the distance from GN  $k$  to the UAV in the  $n$ th time slot,  $\alpha_L$  denotes the path loss exponent for the LoS state. Furthermore,  $d$  is the antenna separation,  $\lambda$  is the carrier wavelength,  $\varphi_k[n]$  and  $\omega_k[n]$  represent the elevation and azimuth angles in the  $n$ th time slot, respectively. Furthermore,  $\sin\varphi_k[n]\cos\omega_k[n] = \frac{x[n]-x_k}{d_k[n]}$  and  $\sin\varphi_k[n]\sin\omega_k[n] = \frac{y[n]-y_k}{d_k[n]}$ . The channel gain between GN  $k$  and the UAV conditioned on the NLoS state in the  $n$ th time slot is given by

$$\mathbf{h}_k^N[n] = \zeta[n]\tilde{\mathbf{h}}_k, \quad (7)$$

where  $\zeta[n] = \sqrt{\beta_0 d_k^{-\alpha_N}[n]}$ ,  $\alpha_N$  denotes the path loss exponent for the NLoS state, and  $\tilde{\mathbf{h}}_k \sim \mathcal{CN}(0, 1)$  is the small-scale fading component modeled by a circularly symmetric complex Gaussian (CSCG) random variable.

<sup>1</sup>Note that the movement of the UAV changes the orientation of the RIS, which will cause the difference between the phase shift designed in this paper and the required phase shift in practice, resulting in performance loss. However, it is reasonable to assume that the RIS can always remain stable in this paper, since we can employ a three-axis gimbal to ensure that the orientation of the RIS keeps unchangeable for the duration of the UAV flight [21].

Assume that GN  $k$  operates in the half-duplex mode, i.e., it can only receive or transmit in each time slot. Thus we define a binary variable that indicates whether GN  $k$  is scheduled to receive reflected signals from the UAV in the  $n$ th time slot or not, i.e., GN  $k$  receives signals from the other GN via the RIS if  $\alpha_k[n] = 1$ , and transmits otherwise. Assume that only one GN is allowed to transmit or receive signals to or from the UAV-borne RIS in the  $n$ th time slot, so we have the following scheduling constraints:

$$\sum_{k=1}^2 \alpha_k[n] \leq 1, \forall n \in \mathcal{N}, \quad (8)$$

$$\alpha_k[n] \in \{0, 1\}, \forall k, n. \quad (9)$$

In a statistical sense, the expected achievable rate in bits/second/Hertz (bps/Hz) from GN  $\bar{k}$  through the UAV to GN  $k$  in the  $n$ th time slot can be given by

$$\begin{aligned} \mathbb{E}[R_k[n]] = & P_k^L[n]P_{\bar{k}}^L[n]R_k^{LL}[n] + P_k^L[n]P_{\bar{k}}^N[n]R_k^{LN}[n] \\ & + P_k^N[n]P_{\bar{k}}^L[n]R_k^{NL}[n] + P_k^N[n]P_{\bar{k}}^N[n]R_k^{NN}[n], \end{aligned} \quad (10)$$

where  $R_k^{f,o}[n] = \log_2 \left( 1 + \gamma_{\bar{k}} \left| \left( \mathbf{h}_k^f[n] \right)^H \Theta[n] \mathbf{h}_{\bar{k}}^o[n] \right|^2 \right)$ ,  $f, o \in \{L, N\}$  denote respectively the achievable rates at GN  $k$  conditioned on the LoS and NLoS states of the air-ground channels. Furthermore,  $\gamma_{\bar{k}} = P_{\bar{k}}/\sigma^2$ , where  $P_{\bar{k}}$  is maximum transmit power of GN  $\bar{k}$  and  $\sigma^2$  is the variance of Gaussian noise at GN  $k$ .

We aim to maximize the minimum average achievable rate by jointly optimizing the communication scheduling  $\mathbf{A}$ , the horizontal UAV trajectory  $\mathbf{Q}$ , the vertical UAV trajectory  $\mathbf{H}$ , and the RIS's phase shift  $\Theta$  for the entire  $N$  time slot. Thus, the optimization problem can be formulated as

$$\max_{\mathbf{A}, \mathbf{Q}, \Theta, \mathbf{H}, \Psi_k} \eta \quad (11a)$$

$$\text{s.t. } \frac{1}{N} \sum_{n=1}^N \alpha_k[n] \mathbb{E}[R_k[n]] \geq \eta, \forall k \in \mathcal{K}, \quad (11b)$$

$$|e^{j\theta_{m_x, m_y}[n]}| = 1, \quad \forall n, \quad (11c)$$

$$(1) - (3), (5), (8) - (9).$$

Problem (11) is non-convex because the rate function  $\bar{R}_k[n]$  in (11b) is not jointly concave with respect to  $\mathbf{A}$ ,  $\Theta$ ,  $\mathbf{Q}$ , and  $\mathbf{H}$ , the binary scheduling constraints in (9) are non-convex, the phase shift constraints in (11c) are non-convex, and the elevation angle constraints in (5) are non-affine, which make it difficult to obtain the optimal solution. In the following section, we propose an efficient iteration algorithm to solve problem (11).

### III. PROPOSED ALGORITHM

In this section, an alternating optimization method<sup>2</sup> is proposed to obtain a high-quality solution to problem (11), where

<sup>2</sup>The optimization algorithm can be executed on a ground control center. Specifically, the ground control center first executes the proposed algorithm and then transmits the optimized variables to the UAV through the control and non-payload communication (CNPC) link so that the UAV can perform the mission according to the designed trajectory [23].

$\mathbf{A}$ ,  $\Theta$ ,  $\mathbf{Q}$ , and  $\mathbf{H}$  are iteratively optimized. Specifically, the original problem is partitioned into three subproblems, each of which is solved in an iterative manner until the algorithm converges.

1) *GNs' Scheduling Optimization*: With any given feasible  $\mathbf{Q}$ ,  $\Theta$ , and  $\mathbf{H}$ , this subproblem can be expressed as

$$\max_{\mathbf{A}, \eta} \eta \quad (12a)$$

$$\text{s.t. } 0 \leq \alpha_k[n] \leq 1, \forall k, n, \quad (12b)$$

$$(8), (11b).$$

Since problem (12) is a standard linear program, it can be solved efficiently by CVX [24].

2) *RIS's Phase Shift Design*: With any given feasible  $\mathbf{A}$ ,  $\mathbf{Q}$ , and  $\mathbf{H}$ , problem (11) can be rewritten as

$$\max_{\Theta, \eta} \eta \quad (13)$$

$$\text{s.t. } (11b) - (11c).$$

Since the constraints (11c) are unit modulus, it is difficult to solve problem (13). To overcome this difficulty, we employ the semidefinite relaxation (SDR). To begin, let us perform the following transformation:

$$\begin{aligned} \left( \mathbf{h}_k^f[n] \right)^H \Theta[n] \mathbf{h}_{\bar{k}}^o[n] = & \left( \mathbf{h}_k^f[n] \right)^H \text{diag}(\mathbf{h}_{\bar{k}}^o[n]) \mathbf{v}[n], \\ & f, o \in \{L, N\}, \end{aligned} \quad (14)$$

where  $\mathbf{v}[n] = [e^{j\theta_{1,1}[n]}, e^{j\theta_{1,2}[n]}, \dots, e^{j\theta_{M_x, M_y}[n]}]^T$ . According to (14), we can reinterpret the square term in the expected achievable rate as

$$\begin{aligned} \left| \left( \mathbf{h}_k^f[n] \right)^H \Theta[n] \mathbf{h}_{\bar{k}}^o[n] \right|^2 = & \left( \mathbf{h}_k^f[n] \right)^H \text{diag}(\mathbf{h}_{\bar{k}}^o[n]) \mathbf{v}[n] \mathbf{v}^H[n] \\ & \text{diag}(\mathbf{h}_{\bar{k}}^o[n])^H \left( \mathbf{h}_k^f[n] \right) = \text{Tr}(\mathbf{V}[n] \mathbf{G}^{f,o}[n]), \quad f, o \in \{L, N\}, \end{aligned} \quad (15)$$

where  $\mathbf{G}^{f,o}[n] = \text{diag}(\mathbf{h}_{\bar{k}}^o[n])^H \left( \mathbf{h}_k^f[n] \right) \left( \mathbf{h}_k^f[n] \right)^H \text{diag}(\mathbf{h}_{\bar{k}}^o[n])$ . Then, the expected achievable rate can be re-expressed as

$$\begin{aligned} \mathbb{E}[\tilde{R}_k[n]] = & P_k^L[n]P_{\bar{k}}^L[n] \log_2 \left( 1 + \text{Tr}(\mathbf{V}[n] \mathbf{G}^{LL}[n]) \right) \\ & + P_k^L[n]P_{\bar{k}}^N[n] \log_2 \left( 1 + \text{Tr}(\mathbf{V}[n] \mathbf{G}^{LN}[n]) \right) \\ & + P_k^N[n]P_{\bar{k}}^L[n] \log_2 \left( 1 + \text{Tr}(\mathbf{V}[n] \mathbf{G}^{NL}[n]) \right) \\ & + P_k^N[n]P_{\bar{k}}^N[n] \log_2 \left( 1 + \text{Tr}(\mathbf{V}[n] \mathbf{G}^{NN}[n]) \right). \end{aligned} \quad (16)$$

Since the expected achievable rate is a function of the newly introduced variable  $\mathbf{V}[n]$ , we can alleviate the difficulties associated with using  $\mathbf{v}[n]$  as the optimization variable. In this respect,  $|\mathbf{v}_{m,m}[n]| = 1$  can be rewritten as  $\mathbf{V}[n] \geq 0$  and

$V_{m,m}[n] = 1$  for the new optimization variable  $V[n]$ . Thus, problem (13) can be rewritten as

$$\max_{\Theta, \eta} \eta \quad (17)$$

$$\text{s.t. } \frac{1}{N} \sum_{n=1}^N \alpha_k[n] \mathbb{E} \left[ \tilde{R}_k[n] \right] \geq \eta, \forall k \in \mathcal{K}, \quad (17a)$$

$$V[n] \geq 0, \quad (17b)$$

$$V_{m,m}[n] = 1, m = 1, 2, \dots, M. \quad (17c)$$

As problem (17) is a semidefinite programming, it can be solved efficiently by CVX. However, a rank-one solution may not be obtained. Hence, we recover  $\mathbf{v}[n]$  from  $V[n]$  using the Gaussian randomization method, which is similar to that in [10] and thus omitted here for brevity.

3) *UAV Horizontal Trajectory Optimization:* With any feasible  $\mathbf{H}$  and  $\mathbf{A}$  and  $\Theta$  obtained by solving problem (12) and (17), respectively, the UAV horizontal trajectory optimization problem can be written as

$$\max_{\mathbf{Q}, \Psi_k, \eta} \eta \quad (18)$$

$$\text{s.t. (1) - (2), (5), (11b).}$$

To facilitate the solution to problem (18), we firstly rewrite Eq. (6) as  $\mathbf{h}_k^L[n] = \tau[n] \mathbf{h}_k^{L'}[n]$ . Note that not only  $\tau[n]$  but also  $\mathbf{h}_k^{L'}[n]$  is relevant to the UAV trajectory. It is observed that  $\mathbf{h}_k^{L'}[n]$  is complex and non-linear with respect to the UAV trajectory variables, which makes the UAV trajectory design intractable. To handle such difficulty, we use the UAV trajectory of the  $(l-1)$  th iteration to obtain an approximate  $\mathbf{h}_k^L[n]$  in the  $l$  th iteration [10]. Therefore, constraint (11b) can be re-expressed as

$$\begin{aligned} & \frac{1}{N} \sum_{n=1}^N \alpha_k[n] \left( P_k^L[n] P_{\bar{k}}^L[n] \log_2 \left( 1 + \xi_k^{LL}[n] d_k^{-\alpha_L}[n] d_{\bar{k}}^{-\alpha_L}[n] \right) \right. \\ & + P_k^L[n] P_{\bar{k}}^N[n] \log_2 \left( 1 + \xi_k^{LN}[n] d_k^{-\alpha_L}[n] d_{\bar{k}}^{-\alpha_N}[n] \right) \\ & + P_k^N[n] P_{\bar{k}}^L[n] \log_2 \left( 1 + \xi_k^{NL}[n] d_k^{-\alpha_N}[n] d_{\bar{k}}^{-\alpha_L}[n] \right) \\ & \left. + P_k^N[n] P_{\bar{k}}^N[n] \log_2 \left( 1 + \xi_k^{NN}[n] d_k^{-\alpha_N}[n] d_{\bar{k}}^{-\alpha_N}[n] \right) \right) \geq \eta, \end{aligned} \quad (19)$$

$$\text{where } \xi_k^{LL}[n] = \frac{p_{\bar{k}} |\beta_0|^2}{\sigma^2} \left| \left( \mathbf{h}_k^{L',(l-1)}[n] \right)^H \Theta[n] \mathbf{h}_k^{L',(l-1)}[n] \right|^2,$$

$$\xi_k^{LN}[n] = \frac{p_{\bar{k}} |\beta_0|^2}{\sigma^2} \left| \left( \mathbf{h}_k^{L',(l-1)}[n] \right)^H \Theta[n] \tilde{\mathbf{h}}_{\bar{k}} \right|^2,$$

$$\xi_k^{NL}[n] = \frac{p_{\bar{k}} |\beta_0|^2}{\sigma^2} \left| \left( \tilde{\mathbf{h}}_{\bar{k}} \right)^H \Theta[n] \mathbf{h}_k^{L',(l-1)}[n] \right|^2,$$

$$\xi_k^{NN}[n] = \frac{p_{\bar{k}} |\beta_0|^2}{\sigma^2} \left| \left( \tilde{\mathbf{h}}_{\bar{k}} \right)^H \Theta[n] \tilde{\mathbf{h}}_{\bar{k}} \right|^2.$$

To deal with the non-convex constraint (19), we introduce the slack variables  $\mathbf{x} = \{x_k[n], \forall k, n\}$ ,  $\mathbf{y} = \{y_k[n], \forall k, n\}$ , and

$\mathbf{z} = \{z_k[n], \forall k, n\}$  into the rate function (11). Thus,  $\mathbb{E} [R_k[n]]$  can be rewritten as

$$\begin{aligned} \mathbb{E} [R_k[n]] &= \frac{1}{x_k[n] x_{\bar{k}}[n]} \log_2 \left( 1 + \frac{\xi_k^{LL}[n]}{y_k^{\alpha_L/2}[n] y_{\bar{k}}^{\alpha_L/2}[n]} \right) \\ &+ \frac{1}{x_k[n] z_{\bar{k}}[n]} \log_2 \left( 1 + \frac{\xi_k^{LN}[n]}{y_k^{\alpha_L/2}[n] y_{\bar{k}}^{\alpha_N/2}[n]} \right) \\ &+ \frac{1}{z_k[n] x_{\bar{k}}[n]} \log_2 \left( 1 + \frac{\xi_k^{NL}[n]}{y_k^{\alpha_N/2}[n] y_{\bar{k}}^{\alpha_L/2}[n]} \right) \\ &+ \frac{1}{z_k[n] z_{\bar{k}}[n]} \log_2 \left( 1 + \frac{\xi_k^{NN}[n]}{y_k^{\alpha_N/2}[n] y_{\bar{k}}^{\alpha_N/2}[n]} \right), \end{aligned} \quad (20)$$

where

$$x_k[n] \geq 1 + a e^{(-b[\psi_k[n]-a])}, \quad (21)$$

$$y_k[n] \geq \|\mathbf{q}[n] - \mathbf{w}_k\|^2 + h[n]^2, \quad (22)$$

$$z_k[n] \geq 1 + \frac{1}{a} e^{(b[\phi_k[n]-a])}. \quad (23)$$

Furthermore,

$$\psi_k[n] \leq \frac{180}{\pi} \arctan \left( \frac{h[n]}{\|\mathbf{q}[n] - \mathbf{w}_k\|} \right), \quad (24)$$

$$\phi_k[n] \geq \frac{180}{\pi} \arctan \left( \frac{h[n]}{\|\mathbf{q}[n] - \mathbf{w}_k\|} \right), \quad (25)$$

are the relaxed constraints for the sake of handling the non-affine constraints (5). We can prove by contradiction that constraints (21)-(25) must hold with equalities to ensure that the objective value of problem (18) does not decrease. Note that, after the variable replacement,  $\tilde{R}_k[n]$  in (20) is jointly convex with respect with  $x_k[n]$ ,  $y_k[n]$ , and  $z_k[n]$ .

Although constraint (24) is non-convex, the right-hand-side (RHS) of (24) is convex with respect to  $\|\mathbf{q}[n] - \mathbf{w}_k\|$ . Since the first-order Taylor approximation of a convex function is a global underestimator, it can be applied at any local points  $x_k^{(l)}[n]$ ,  $y_k^{(l)}[n]$ ,  $z_k^{(l)}[n]$ , and  $\|\mathbf{q}^{(l)}[n] - \mathbf{w}_k\|$  in the  $l$ th iteration for (20) and (24), i.e., (26) which is shown at the top of the next page, and

$$\begin{aligned} \psi_k[n] &\leq \frac{180}{\pi} \arctan \left( \frac{h[n]}{\|\mathbf{q}[n] - \mathbf{w}_k\|} \right) \\ &= \frac{180}{\pi} \left( F_k^{(l)}[n] - G_k^{(l)}[n] \left( \|\mathbf{q}[n] - \mathbf{w}_k\| - \|\mathbf{q}^{(l)}[n] - \mathbf{w}_k\| \right) \right), \end{aligned} \quad (27)$$

$$\text{where } B^{(l)}[n] = 1 + \frac{\xi_k^{LL}[n]}{\left( y_k^{(l)}[n] \right)^{\alpha_L/2} \left( y_{\bar{k}}^{(l)}[n] \right)^{\alpha_L/2}}, \quad C^{(l)}[n] = 1 +$$

$$\frac{\xi_k^{LN}[n]}{\left( y_k^{(l)}[n] \right)^{\alpha_L/2} \left( y_{\bar{k}}^{(l)}[n] \right)^{\alpha_N/2}}, \quad D^{(l)}[n] = 1 + \frac{\xi_k^{NL}[n]}{\left( y_k^{(l)}[n] \right)^{\alpha_N/2} \left( y_{\bar{k}}^{(l)}[n] \right)^{\alpha_L/2}},$$

$$\text{and } E^{(l)}[n] = 1 + \frac{\xi_k^{NN}[n]}{\left( y_k^{(l)}[n] \right)^{\alpha_N/2} \left( y_{\bar{k}}^{(l)}[n] \right)^{\alpha_N/2}}. \quad \text{Furthermore,}$$

$$F_k^{(l)}[n] = \arctan \left( \frac{h[n]}{\|\mathbf{q}^{(l)}[n] - \mathbf{w}_k\|} \right) \quad \text{and} \quad G_k^{(l)}[n] = \frac{h[n]}{\|\mathbf{q}^{(l)}[n] - \mathbf{w}_k\|^2 + H^2}.$$



$$\begin{aligned}
& \frac{\log_2(B^{(l)}[n])}{x_k^{(l)}[n]x_{\bar{k}}^{(l)}[n]} + \frac{\log_2(C^{(l)}[n])}{x_k^{(l)}[n]z_{\bar{k}}^{(l)}[n]} + \frac{\log_2(D^{(l)}[n])}{z_k^{(l)}[n]x_{\bar{k}}^{(l)}[n]} + \frac{\log_2(E^{(l)}[n])}{z_k^{(l)}[n]z_{\bar{k}}^{(l)}[n]} - \left( \frac{\log_2(B^{(l)}[n])}{x_k^{(l)}[n](x_{\bar{k}}^{(l)}[n])^2} + \frac{\log_2(D^{(l)}[n])}{z_k^{(l)}[n](x_{\bar{k}}^{(l)}[n])^2} \right) (x_{\bar{k}}[n] - x_{\bar{k}}^{(l)}[n]) - \left( \frac{\log_2(B^{(l)}[n])}{(x_{\bar{k}}^{(l)}[n])^2} \frac{x_{\bar{k}}^{(l)}[n]}{x_{\bar{k}}^{(l)}[n]} \right. \\
& + \left. \frac{\log_2(C^{(l)}[n])}{(x_{\bar{k}}^{(l)}[n])^2} \frac{z_{\bar{k}}^{(l)}[n]}{z_{\bar{k}}^{(l)}[n]} \right) (x_k[n] - x_k^{(l)}[n]) - \left( \frac{\log_2(C^{(l)}[n])}{x_k^{(l)}[n](z_{\bar{k}}^{(l)}[n])^2} + \frac{\log_2(E^{(l)}[n])}{z_k^{(l)}[n](z_{\bar{k}}^{(l)}[n])^2} \right) (z_{\bar{k}}[n] - z_{\bar{k}}^{(l)}[n]) - \left( \frac{\log_2(D^{(l)}[n])}{x_k^{(l)}[n](z_{\bar{k}}^{(l)}[n])^2} + \frac{\log_2(E^{(l)}[n])}{z_k^{(l)}[n](z_{\bar{k}}^{(l)}[n])^2} \right) (z_k[n] \\
& - z_k^{(l)}[n]) - \left( \frac{\alpha_L \xi_k^{LL}[n] (y_k^{(l)}[n])^{-\frac{\alpha_L-1}{2}} \log_2 e}{2x_k^{(l)}[n]x_{\bar{k}}^{(l)}[n] (y_k^{(l)}[n])^{\frac{\alpha_L}{2}} B^{(l)}[n]} + \frac{\alpha_L \xi_k^{LN}[n] (y_k^{(l)}[n])^{-\frac{\alpha_L-1}{2}} \log_2 e}{2x_k^{(l)}[n]z_{\bar{k}}^{(l)}[n] (y_k^{(l)}[n])^{\frac{\alpha_L}{2}} C^{(l)}[n]} + \frac{\alpha_N \xi_k^{NL}[n] (y_k^{(l)}[n])^{-\frac{\alpha_N-1}{2}} \log_2 e}{2z_k^{(l)}[n]x_{\bar{k}}^{(l)}[n] (y_k^{(l)}[n])^{\frac{\alpha_N}{2}} D^{(l)}[n]} \right. \\
& + \left. \frac{\alpha_N \xi_k^{NN}[n] (y_k^{(l)}[n])^{-\frac{\alpha_N-1}{2}} \log_2 e}{2z_k^{(l)}[n]z_{\bar{k}}^{(l)}[n] (y_k^{(l)}[n])^{\frac{\alpha_N}{2}} E^{(l)}[n]} \right) (y_k[n] - y_k^{(l)}[n]) - \left( \frac{\alpha_L \xi_k^{LL}[n] (y_k^{(l)}[n])^{-\frac{\alpha_L-1}{2}} \log_2 e}{2x_k^{(l)}[n]x_{\bar{k}}^{(l)}[n] (y_k^{(l)}[n])^{\frac{\alpha_L}{2}} B^{(l)}[n]} + \frac{\alpha_N \xi_k^{LN}[n] (y_k^{(l)}[n])^{-\frac{\alpha_N-1}{2}} \log_2 e}{2x_k^{(l)}[n]z_{\bar{k}}^{(l)}[n] (y_k^{(l)}[n])^{\frac{\alpha_L}{2}} C^{(l)}[n]} \right. \\
& + \left. \frac{\alpha_L \xi_k^{NL}[n] (y_k^{(l)}[n])^{-\frac{\alpha_L-1}{2}} \log_2 e}{2z_k^{(l)}[n]x_{\bar{k}}^{(l)}[n] (y_k^{(l)}[n])^{\frac{\alpha_N}{2}} D^{(l)}[n]} + \frac{\alpha_N \xi_k^{NN}[n] (y_k^{(l)}[n])^{-\frac{\alpha_N-1}{2}} \log_2 e}{2z_k^{(l)}[n]z_{\bar{k}}^{(l)}[n] (y_k^{(l)}[n])^{\frac{\alpha_N}{2}} E^{(l)}[n]} \right) (y_{\bar{k}}[n] - y_{\bar{k}}^{(l)}[n]), \tag{26}
\end{aligned}$$

With (26)-(27), problem (18) can be reformulated into the following convex optimization problem,

$$\begin{aligned}
& \max_{\mathbf{Q}, \Psi_k, \Phi_k, \mathbf{x}_k, \mathbf{z}_k, \mathbf{y}_k, \eta} \eta \\
& \text{s.t. (1) - (2), (21) - (23), (25) - (27),} \tag{28}
\end{aligned}$$

where  $\Psi_k = \{\psi_k[n], \forall k, n\}$  and  $\Phi_k = \{\phi_k[n], \forall k, n\}$ . As such, problem (28) can be efficiently solved by CVX [24].

4) *UAV Vertical Trajectory Optimization:* With the optimal  $\mathbf{A}$ ,  $\mathbf{Q}$ , and  $\Theta$  obtained by problem (12), (17), and (28), the UAV vertical trajectory optimization problem can be reformulated as

$$\begin{aligned}
& \max_{\mathbf{H}, \Psi_k, \eta} \eta \\
& \text{s.t. (3), (5), (11b),} \tag{29}
\end{aligned}$$

Since problems (18) and (29) are similar in form and differ only slightly in terms of optimization variables  $\mathbf{H}$ , the procedure for solving problem (18) can be similarly applied to solve problem (29). We omit the detailed derivation owing to the page limitation.

5) *Overall Algorithm:* By applying our proposed algorithm, problem (15) can be solved by alternately optimizing variables  $\mathbf{A}$ ,  $\Theta$ ,  $\mathbf{Q}$ , and  $\mathbf{H}$ , while its solution converges to a preset accuracy  $\epsilon$ . Note that the binary solution can be reconstructed with high precision from the obtained continuous variables of GN's transmission scheduling by applying the proposed reconstruction method in [4]. Since the four subproblems are solved by applying CVX via the standard interior point method, their computational complexity can be obtained as  $O_1((KN)^{3.5} \log(1/\epsilon))$ ,  $O_2(\sqrt{M} \log(1/\epsilon) ((KN+1)M^3 + (KN+1)^2 M^2 + (KN+1)^3))$ ,  $O_3((2N+6KN)^{3.5} \log(1/\epsilon))$ , and  $O_4((2N+6KN)^{3.5} \log(1/\epsilon))$ , respectively. Thus, the total computational complexity of our proposed algorithm is in the order of  $O_1 + O_2 + O_3 + O_4$ .

#### IV. SIMULATION RESULTS

In this section, we provide simulation results to show the interesting elevation angle and distance trade-off of the 3D

UAV trajectory design under the PLC model (denoted as PLC for brevity). The following schemes are used for comparison: 1) UAV horizontal trajectory design under the PLC scheme with fixed altitude being  $H = 200$  m (denoted as PLCFA); 2) 3D UAV trajectory design under the LC model (denoted as DLC). We assume that GN1 and GN 2 are located at (0, 0, 0) m and (800, 0, 0) m, respectively. Unless otherwise stated, the simulation results are set as:  $\hat{v}_{max} = 40$  m/s,  $\tilde{v}_{max} = 20$  m/s,  $p_1 = p_2 = 0.1$  W,  $\beta_0 = -40$  dB,  $H_{min} = 100$  m,  $H_{max} = 500$  m,  $d = \frac{\lambda}{2}$ ,  $\sigma^2 = -169$  dBm,  $\alpha_L = 2.2$ ,  $\alpha_N = 3.2$ ,  $a = 11.95$ , and  $b = 0.14$  [17], [18]. Furthermore, the initialized trajectory of the UAV is set to be a straight-line trajectory with a fix altitude  $H = 200$  m, i.e., the UAV flies from  $\mathbf{q}_0 = [-200, -200]$  to  $\mathbf{q}_F = [1000, 200]$  at its maximum flying speed.

Fig. 2 shows the different 3D UAV trajectories by three schemes with  $T = 150$  s. It can be seen that the UAV in the DLC first descends quickly to  $H_{min}$ , hovers over GN 1, then flies horizontally at its maximum speed, and hovers over GN 2. Finally, the UAV rises and flies back to the final location. This is because hovering above each GN at  $H_{min}$  suffers from the least path loss for the cascade channel between the UAV and the GNs. By contrast, in the PLC scheme, the UAV first ascends rapidly to increase the elevation angle between the UAV and each GN for a higher LoS probability. Then, the UAV hovers above the midpoint of the two GNs, which results in less path loss while maintaining a larger LoS probability of the cascaded channel. Compared to the PLC scheme that the UAV hovers only above the midpoints of the two GNs, the UAV in the PLCFA scheme hovers close to both sides of the midpoint of the two GNs. This is because that although hovering at the midpoint of the two GNs can maximize the LoS probability of the cascaded channel, i.e.,  $P_k^L[n]P_{\bar{k}}^L[n]$ , the larger path loss of the communication links also degrades the rate performance. Therefore, our proposed PLC scheme can take advantage of the additional design brought by the UAV vertical trajectory to obtain a more efficient angle-distance trade-off than the PLCFA scheme.

Fig. 3 illustrates the achieved expected max-min rates of different schemes versus  $T$  when  $M = 100$ . It can be seen

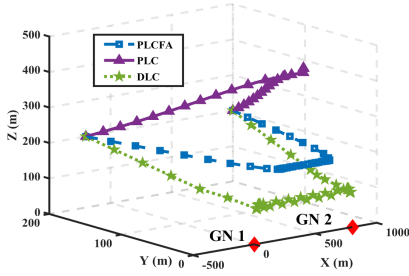
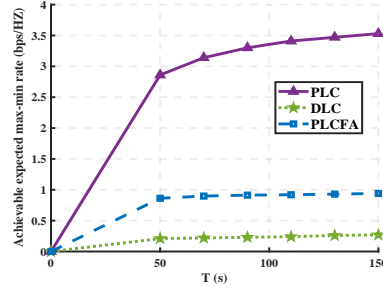
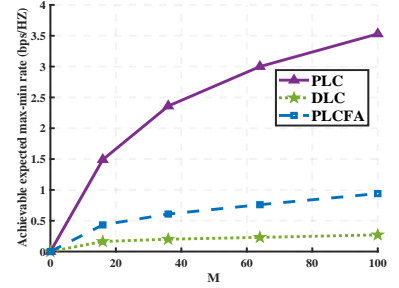


Fig. 1: UAV's trajectories.

Fig. 2: Achieved expected max-min rate versus  $T$ .Fig. 3: Achieved expected max-min rate versus  $M$ .

that the PLCFA scheme achieves larger rates than the DLC scheme, which indicates the necessity of adopting the more accurate PLC model to describe the LoS/NLoS channel states in the UAV-borne RIS communication system. Furthermore, our proposed PLC scheme significantly improves performance over the PLCFA scheme. The reason is that the additionally designing the UAV vertical trajectory can further increase the LoS probability of the cascaded channel. Fig. 4 shows the achieved expected max-min rates for different schemes with  $T = 150$  s versus different  $M$ . As expected, the rate performance is significantly increased when more elements are equipped in the RIS due to the larger passive beamforming gain. In practice, we cannot increase  $M$  indefinitely to obtain higher rates due to the limitation of the size of rotary-wing UAVs. An oversized  $M$  will result in a larger RIS size, which will increase the weight of the UAV and result in greater energy consumption (i.e., shorter endurance). Therefore, an interesting trade-off exists between  $M$  (i.e., related to the RIS size) and the UAV energy consumption for rate improvement.

## V. CONCLUSION

This paper investigated the potential of rate enhancement for the aerial RIS-aided communication system under the accurate PLC model in the dense urban environment. The objective was to maximize the minimum average achievable rate. We proposed an efficient iterative algorithm to jointly optimize the communication schedule, the RIS's phase shift, and the 3D UAV trajectory. Numerical results showed that the proposed scheme has a significant improvement compared to the conventional DLC scheme. Furthermore, our proposed scheme enjoys the additional gain of elevation angle-dependent 3D UAV trajectory design and can effectively balance the elevation angle and distance trade-off between the UAV and the GNs, whereas the DLC scheme cannot. This validates the practical importance of considering the more accurate PLC model to support UAV-borne RIS communications in urban environments.

Note that in the suburban/urban/dense urban environment, the error in the approximated PLC model [22] is extremely small and thus can be ignored. However, this PLC model suffers from errors in the high-rise urban environment, which may cause performance loss. In this case, the hybrid *offline-online* 3D UAV trajectory design proposed in [17] may be an alternative to better characterize the real-time location-dependent air-ground channel states, which is interesting to

study whether the performance loss can be further compensated by employing additional online design.

## REFERENCES

- [1] Y. Zeng, Q. Wu, and R. Zhang, "Accessing from the sky: A tutorial on UAV communications for 5G and beyond," *Proc. IEEE*, vol. 107, no. 12, pp. 2327–2375, 2019.
- [2] R. Zhou, X. Zhang, X. Wang, G. Yang, H.-N. Dai, and M. Liu, "Device-oriented keyword searchable encryption scheme for cloud-assisted industrial IoT," *IEEE Internet Things J.*, pp. 1–1, 2021.
- [3] G. Zhang, Q. Wu, M. Cui, and R. Zhang, "Securing UAV communications via joint trajectory and power control," *IEEE Trans. Wireless Commun.*, vol. 18, no. 2, pp. 1376–1389, 2019.
- [4] Q. Wu, Y. Zeng, and R. Zhang, "Joint trajectory and communication design for Multi-UAV enabled wireless networks," *IEEE Trans. Wireless Commun.*, vol. 17, no. 3, pp. 2109–2121, 2018.
- [5] B. Duo, Q. Wu, X. Yuan, and R. Zhang, "Energy efficiency maximization for full-duplex UAV secrecy communication," *IEEE Trans. Veh. Technol.*, vol. 69, no. 4, pp. 4590–4595, 2020.
- [6] Q. Wu and R. Zhang, "Towards smart and reconfigurable environment: Intelligent reflecting surface aided wireless network," *IEEE Trans. Commun.*, vol. 58, no. 1, pp. 106–112, 2020.
- [7] Q. Wu and R. Zhang, "Intelligent reflecting surface enhanced wireless network via joint active and passive beamforming," *IEEE Trans. Wireless Commun.*, vol. 18, no. 11, pp. 5394–5409, 2019.
- [8] L. Yang, F. Meng, J. Zhang, M. O. Hasna, and M. D. Renzo, "On the performance of RIS-assisted dual-hop UAV communication systems," *IEEE Trans. Veh. Technol.*, vol. 69, no. 9, pp. 10385–10390, 2020.
- [9] X. Liu, Y. Liu, and Y. Chen, "Machine learning empowered trajectory and passive beamforming design in UAV-RIS wireless networks," *IEEE J. Select. Areas Commun.*, vol. 39, no. 7, pp. 2042–2055, 2021.
- [10] S. Li, B. Duo *et al.*, "Robust secure UAV communications with the aid of reconfigurable intelligent surfaces," *IEEE Trans. Wireless Commun.*, pp. 1–1, 2021.
- [11] S. Li *et al.*, "Reconfigurable intelligent surface assisted UAV communication: Joint trajectory design and passive beamforming," *IEEE Wireless Commun. Lett.*, vol. 9, no. 5, pp. 716–720, 2020.
- [12] A. S. Abdalla *et al.*, "UAVs with reconfigurable intelligent surfaces: Applications, challenges, and opportunities," 2020. [Online]. Available: <https://arxiv.org/abs/2012.04775>
- [13] B. Shang, R. Shafin, and L. Liu, "UAV swarm-enabled aerial reconfigurable intelligent surface," 2021. [Online]. Available: <https://arxiv.org/abs/2103.06361>
- [14] H. Lu *et al.*, "Aerial intelligent reflecting surface: Joint placement and passive beamforming design with 3D beam flattening," *IEEE Trans. Wireless Commun.*, vol. 20, no. 7, pp. 4128–4143, 2021.
- [15] S. Jiao *et al.*, "Joint beamforming and phase shift design in downlink UAV networks with IRS-assisted NOMA," *J. Commun. Inf. Networks*, vol. 5, no. 2, pp. 138–149, 2020.
- [16] H. Long *et al.*, "Reflections in the sky: Joint trajectory and passive beamforming design for secure UAV networks with reconfigurable intelligent surface," 2020. [Online]. Available: <https://arxiv.org/abs/2005.10559>
- [17] C. You and R. Zhang, "Hybrid offline-online design for UAV-enabled data harvesting in probabilistic LoS channels," *IEEE Trans. Wireless Commun.*, vol. 19, no. 6, pp. 3753–3768, 2020.
- [18] B. Duo *et al.*, "Anti-jamming 3D trajectory design for UAV-enabled wireless sensor networks under probabilistic LoS channel," *IEEE Trans. Veh. Technol.*, vol. 69, no. 12, pp. 16288–16293, 2020.

- [19] T. Shafique *et al.*, “Optimization of wireless relaying with flexible UAV-borne reflecting surfaces,” *IEEE Trans. Commun.*, vol. 69, no. 1, pp. 309–325, 2021.
- [20] A. Mahmoud *et al.*, “Intelligent reflecting surfaces assisted UAV communications for IoT networks: Performance analysis,” *IEEE Trans. Green Commun. Networking*, vol. 5, no. 3, pp. 1029–1040, 2021.
- [21] F. Zhang, “Simultaneous self-calibration of nonorthogonality and non-linearity of cost-effective multiaxis inertially stabilized gimbal systems,” *IEEE Rob. Autom. Lett.*, vol. 3, no. 1, pp. 132–139, 2018.
- [22] A. Al-Hourani *et al.*, “Optimal LAP altitude for maximum coverage,” *IEEE Wireless Commun. Lett.*, vol. 3, no. 6, pp. 569–572, 2014.
- [23] B. Duo, H. Hu, Y. Li, Y. Hu, and X. Zhu, “Robust 3D trajectory and power design in probabilistic LoS channel for UAV-enabled cooperative jamming,” *Veh. Commun.*, vol. 32, p. 100387, 2021.
- [24] B. S. Grant, M. CVX: Matlab Software for Disciplined Convex Programming, Version 2.2. (2020). [Online]. Available: <http://cvxr.com/cvx>